RSC Advances

PAPER

View Article Online
View Journal | View Issue

Cite this: *RSC Adv.*, 2017, **7**, 46796

Synthesis and characterization of $SrSnO_3$ doped with Er^{3+} for up-conversion luminescence temperature sensors

E. Cortés-Adasme,[a] M. Vega,[*ab] I. R. Martin[c] and J. Llanos[a]

Received 3rd August 2017
Accepted 27th September 2017

DOI: 10.1039/c7ra08603b

rsc.li/rsc-advances

The present work shows the results of the synthesis of $SrSnO_3$:Er^{3+} (doped from 0% to 7% with Er^{3+}) prepared using a sol–gel method. Structural studies based on powder X-ray diffraction (XRD) showed that the compounds crystallize in an orthorhombic perovskite type structure (space group: *Pbnm*). The infrared spectra (IR) of Er_2O_3, $SrSnO_3$ and $SrSnO_3$:Er (1%) were measured in the range of 400–1000 cm^{-1}, which confirmed the octahedral tilting of SnO_6. The dependence of the green and red up-conversion (UC) emission bands on the pump power have been investigated using NIR (975 nm) laser irradiation. The decay curve was collected to determine the plausible mechanisms of the UC green emission, which showed that a Ground-State Absorption/Excited-State Absorption (GSA/ESA) process involving two photons was the indicated mechanism for this emission. The optical temperature sensing properties were investigated using the fluorescence intensity ratio technique (FIR) for the green UC emission. The temperature dependence of the green emissions at 528 nm ($^2H_{11/2} \rightarrow {}^4I_{15/2}$) and 549 nm ($^4S_{3/2} \rightarrow {}^4I_{15/2}$) were investigated. The maximum temperature sensitivity over the range of 294–372 K was 7.91 × 10^{-3} K^{-1} at 368 K, and the sensor sensitivity was 9.97 × 10^{-3} K^{-1} at 294 K. The results suggest that Er^{3+} doped $SrSnO_3$ is a promising material for optical temperature sensors for biological processes.

1. Introduction

Recently, the temperature-dependent up-conversion luminescence of materials doped with lanthanide ions has drawn considerable attention because of the potential application in thermal imaging, cancer treatment, temperature sensors and optical heaters.[1,2] Non-invasive optical temperature sensors based on up-conversion emission are one of the most important applications. In these sensors, the temperature is measured using the fluorescence intensity ratio (FIR) technique. This technique involves a comparison of the fluorescence intensities from two thermally coupled energy levels (TCEL).[3] The FIR technique plays a key role because of its high resolution and the independence of the measurement compared to other optical-based techniques, such as fluorescence lifetime and amplified spontaneous emission.[1,4] Many materials doped/co-doped with rare earth ions, such as Pr^{3+}, Dy^{3+}, Nd^{3+}, Sm^{3+}, Ho^{3+}, Tm^{3+}, Yb^{3+} and Eu^{3+}, have been studied for temperature sensing based on the change in the FIR of two thermally coupled levels as a function of temperature.[5,6] TCELs with large energy gaps are required for high temperature sensitivity. However, when the gap between these two close levels increases to a certain point, the population of ions between these two levels, by inter-relaxation, tends to slow down exponentially with the gap, in consequence the thermal-coupling begins to fade when the rates are no longer much faster than the relaxation rates to outside levels.[7] Among the trivalent rare earth ions, temperature sensors based on the green up-converted luminescence of Er^{3+} are the most popular because they exhibit up-conversion fluorescence emissions upon excitation using infrared (IR) radiation and the erbium ions have a thermally coupled pair of energy levels, $^2H_{11/2}$ and $^4S_{3/2}$,[8] whose populations follow the Boltzmann distribution law. The temperature can be obtained using the fluorescence intensity ratio (FIR) technique. The fluorescence intensity ratio of luminescence bands corresponding to the $^2H_{11/2} \rightarrow {}^4I_{15/2}$ and $^4S_{3/2} \rightarrow {}^4I_{15/2}$ transitions of Er^{3+} fulfill a temperature-dependent function, because the energy gap between the two thermally coupled excited states, $^2H_{11/2}$ and $^4S_{3/2}$, is quite small (approximately 800 cm^{-1}). The relative fluorescence intensity of the two green bands of the Er^{3+} ion varies substantially with temperature, whereas their spectral positions remain the same. This feature is often used for temperature measurements.[9]

To the best of our knowledge, $SnSrO_3$ has not been used as a host structure for the Er^{3+} cation for use as temperature

[a]*Departamento de Química, Universidad Católica del Norte, Avenida Angamos 0610, Antofagasta, Chile. E-mail: mvega02@ucn.cl; Tel: +56 55 235 5606*

[b]*Departamento de Química, Facultad de Ciencias, Universidad de Chile, Casilla 635, Santiago, Chile*

[c]*Departamento de Física, Instituto de Materiales y Nanotecnología (IMN), Universidad de La Laguna, 38206 La Laguna, Tenerife, Spain*

sensor. In this paper, we report on the synthesis of $Sr_{1-x}Er_x$-$SnO_{3-\delta}$ *via* a modified sol–gel process and its application as a temperature sensor. The up-conversion mechanism is also investigated.

2. Experimental

2.1. Synthesis

The starting materials $SrCO_3$ (99.99%, Aldrich), $SnCl_2 \cdot 2H_2O$ (98%, Aldrich) and Er_2O_3 (99.99%, Aldrich) were purchased from Aldrich Chemical Co. and used as received.

Solid solutions of the $Sr_{1-x}Er_xSnO_{3-\delta}$ ($x = 0.01$, 0.03, 0.04, 0.05 and 0.07) system were prepared using the method described by Ouni *et al.*[10] Stoichiometric quantities of Er_2O_3, $SrCO_3$, and $SnCl_2 \cdot 2H_2O$ were dissolved in 150 ml of a 1 : 2 solution of hydrochloric acid and distilled water. Then, 5 ml of ethylene glycol (99.99%, Aldrich) and one equivalent of citric acid per mole of M^{3+} cation (99.99%, Aldrich) were added and the solution was heated on a hot plate at 353 K with constant stirring for approximately 6 h.

The obtained transparent gel was decomposed by heating at 523 K for 3 h. The resulting fine dark powder was ground up and then placed in a muffle furnace in air at 1173 K for 6 h resulting in the formation of the final white powder.

2.2. Characterization

Powder X-ray diffraction (XRD) was performed using the Bruker AXS D8 Advance diffractometer in the range from 10° to 60°, with a graphite monochromator using CuKα radiation (λ = 1.54057 Å) operating at 40 kV and 30 mA. The sample images were obtained using a TESCAN VEGA3 SB model scanning electron microscope. Infrared spectroscopy was performed using a FRONTIER IR spectrophotometer from Perkin Elmer. The up-conversion spectra were obtained by exciting the samples using a titanium-sapphire laser (λ = 975 nm) pumped by a Millennia laser (λ = 532 nm) with a maximum power of 15 W. The laser was focused on the sample using a lens with a focal length of 30 mm. The emitted light was focused on the slit door of the CCD spectrograph (ANDOR SHAMROCK 303i) using a lens with a focal length of 50 mm. The luminescence decay curves were obtained by exciting the samples using an OPO pulsed laser (EKSPLA/NT342/3/UVE). The emission was focused on the input of a spectrograph coupled to a photomultiplier (R928 HAMAMATSU in the visible range) connected to a digital oscilloscope (TEKTRONIX 2430). The temperature-dependent luminescence measurements were performed in an electric tube furnace (GERO RES-E 230/3) from 294 K to 374 K. The sample was placed in the center of the furnace and heated at a rate of 1 K min^{-1}. The sample was excited with laser radiation at 488 nm from argon laser.

3. Results and discussion

3.1. Powder X-ray diffraction

The X-ray diffraction patterns for the series of $SrSnO_3$ powders doped with Er^{3+} (1%, 3%, 5% and 7%) were analyzed and are shown in Fig. 1. All samples were indexed to the distorted orthorhombic perovskite with the space group *Pbnm*. Inspection of the X-ray diffraction patterns at intermediate phases of the synthesis appeared to indicate the formation of not only the $SrSnO_3$ perovskite type structure but also minor impurity phases of SnO_2 and Er_2O_3, as shown in Fig. 1. It is important to note that according to the literature, the synthesis of $SrSnO_3$ is never pure and always contains some impurities, as shown in other studies.[10,11] In the structure of $SrSnO_3$, the Sr^{2+} and Sn^{4+} occupy only one crystallographic site, respectively. The Sn^{4+} is six-fold coordinated by oxygen atoms, whereas the Sr^{2+} is twelve-fold coordinated by oxygen atoms. Upon doping, the trivalent erbium ions are expected to occupy the Sn^{4+} sites, since the ionic radius of Er^{3+} $r = 0.89$ Å (CN = 6) is slightly larger than the ionic radius of Sn^{4+} $r = 0.69$ Å (CN = 6). Due to the ionic radius of Sr^{2+} r = 1.44 Å (CN = 12) is larger than that of Er^{3+}, the replacement of the Sr^{2+} ions by Er^{3+} can results in a strong contraction of the unit cell.[12] Our results show that the unit cell parameters of $SrSnO_3$:Er^{3+} increase with the increasing of Er^{3+} concentration, this fact should be explained by the replacement of the Sn^{4+} cations by the rare-earth ions. Although the Goldschmidt's tolerance factor is compatible with the replacement of Sr^{2+} or Sn^{4+} in order to retain the orthorhombic structure of the host matrix.[13] The value of the cell parameters, confirmed by Le Bail refinement[14,15] for all compounds, using the program JANA2006,[16] are given in Table 1. When increasing the Er concentration to 5%, the previously named impurities began to appear as shown in Fig. 1, this implies that the maximum solubility of the Er ion in $SrSnO_3$ is approximately 3%.[10] We can conclude then, that due to the impurities formation, Er ions

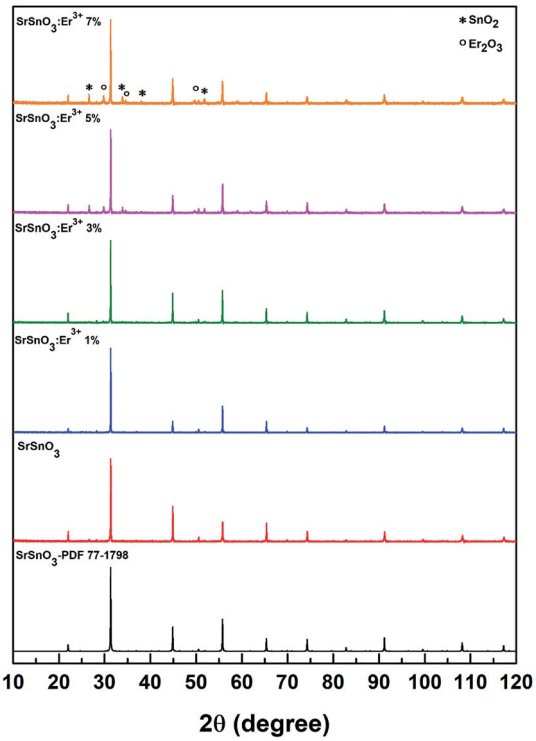

Fig. 1 XRD patterns of the $SrSnO_3$ doped with different content of Er^{3+}.

Table 1 Unit cell volume and lattice parameters for $SrSnO_3$ doped with Er^3 ions up to 7%

Samples	a (Å)	b (Å)	c (Å)	Vol. (Å^3)
Er1%	5.7212(5)	5.7056(1)	8.0681(2)	263.37(0)
Er3%	5.7228(5)	5.7069(1)	8.0721(2)	263.63(0)
Er5%	5.7285(7)	5.7042(1)	8.0680(2)	263.63(0)
Er7%	5.7412(7)	5.7061(2)	8.0699(3)	264.37(0)

does not occupied a place in the structure but rather begins to form these new compounds.

3.2. Infrared spectra

The IR spectra of the doped and undoped samples of $SrSnO_3$ are shown in Fig. 2a and b, respectively, along with the spectra of the Er_2O_3. The obtained powders were pulverized, mixed with KBr and then pressed into fine pellets.

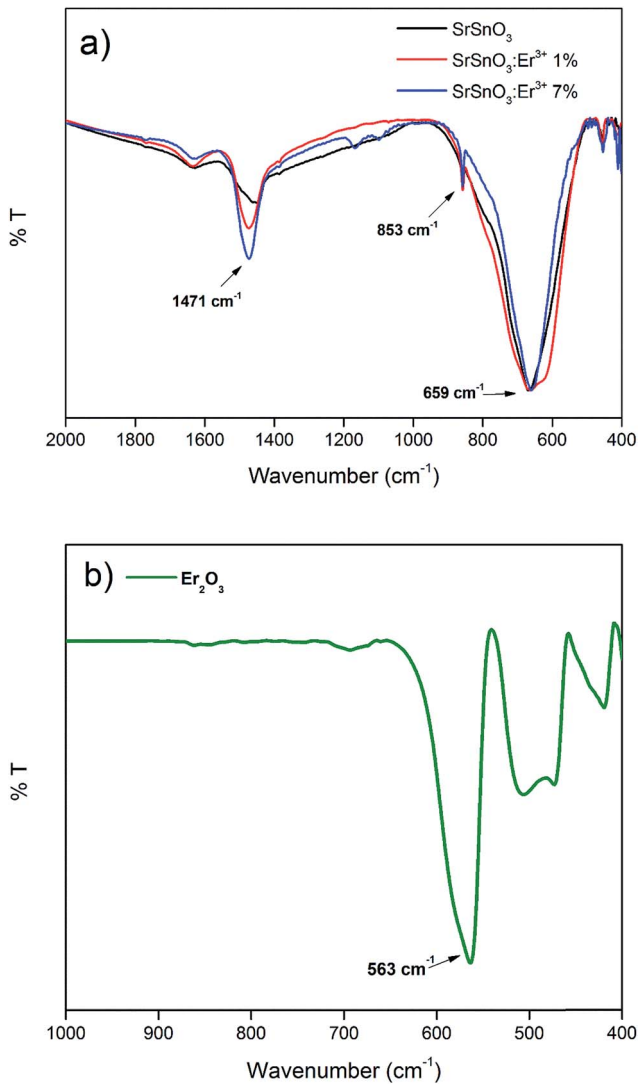

Fig. 2 IR spectrum of (a) $SrSnO_3$ un-doped and doped with 1% and 7% of Er^{3+} and (b) Er_2O_3.

The IR bands below 1000 cm^{-1} are generally attributed to the deformation modes of Sn–O bonds in SnO_6 octahedra or the deformation of Sn–O–Sn bridges.[17] The vibration of the stannate (SnO_3^{2-}) group produced high intensity bands in the ranges of 300–400 cm^{-1} and 600–700 cm^{-1}.[18] The IR spectrum of Er_2O_3 shows a band at 563 cm^{-1}, which corresponds to Er–O vibrations originating from the octahedral coordination ErO_6. By comparing this spectrum with the spectra of the different synthesized phases, it is obvious that this band is absent. Due to the concentrations of Er^{3+} ions are so low we are unable to detect the band corresponding to the Er–O vibrations, although the Er^{3+} ions replace the Sn^{4+} ions in the host structure.

3.3. Scanning electron microscopy

The SEM image of the $SrSnO_3$:Er^{3+} 1% doping, is shown in Fig. 3. The image was generated using backscattered electrons (BSE). The main observation from these images is the formation of micron-sized agglomerates which lack a defined morphology.

3.4. Up-conversion emission

The room temperature UC spectra of the doped samples with different concentrations of the Er^{3+} ions are shown in Fig. 4. All spectra were obtained using a 975 nm excitation. The emission spectra of the $SrSnO_3$:Er^{3+} phosphors exhibit strong emission bands at 528 and 549 nm and a weak emission at 665 nm, which correspond to the $^2H_{11/2} \rightarrow {}^4I_{15/2}$, $^4S_{3/2} \rightarrow {}^4I_{15/2}$ and $^4F_{9/2} \rightarrow {}^4I_{15/2}$ electronic transitions of the Er^{3+} ion, respectively. The UC emission intensity decreases as the concentration of the Er^{3+} ion increases. The intensity of the emission band at 528 nm is higher than the emission band at 549 nm at high concentration of Er^{3+} (7%) in the $SrSnO_3$ host structure. This could be explained because of, at high concentration of Er^{3+} ions (7%),

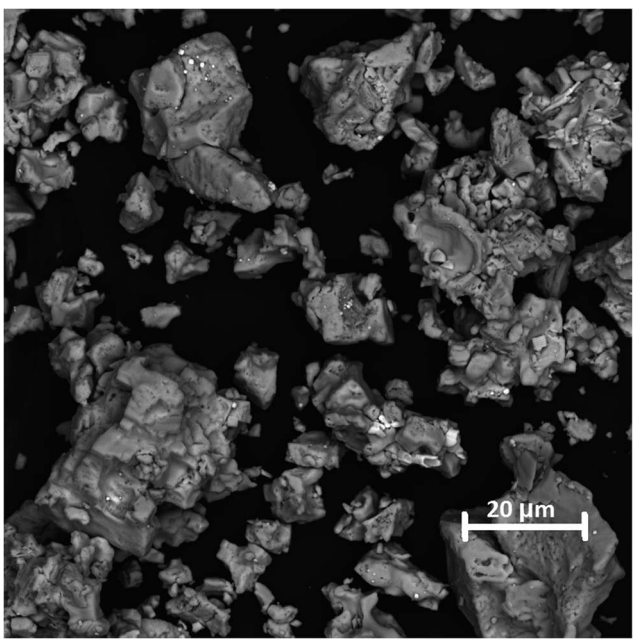

Fig. 3 SEM micrography of $SrSnO_3$ doped up to 1% of Er^{3+}.

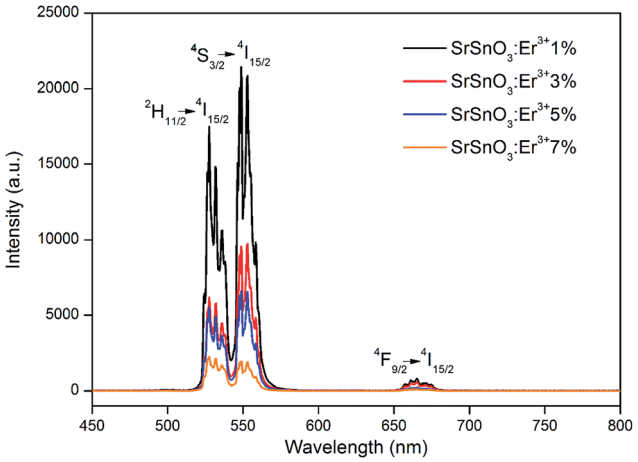

Fig. 4 Up-conversion spectra emission of the $SrSnO_3$ doped with Er^{3+} from 1% to 7%, exciting at 975 nm.

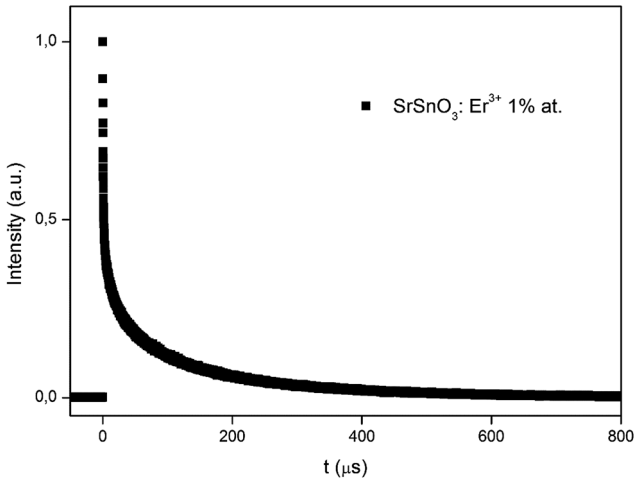

Fig. 6 Temporal evolution of the up-conversion emission at 549 nm of the $SrSnO_3$ doped with 1% of Er^{3+} for excitation at 975 nm.

Er_2O_3 impurities became more important, resulting in a higher emission band at 528 nm. This could be explained because the $^2H_{11/2} \rightarrow {}^4I_{15/2}$ transition of the Er_2O_3 begins to interfere with the emission spectra of the $SrSnO_3$:Er^{3+} doped structure. The dominance of the $^2H_{11/2} \rightarrow {}^4I_{15/2}$ transition in the Er_2O_3 structure was reported recently by Tabanli *et al.*[19]

To determine the mechanism behind photon UC in $SrSnO_3$:Er^{3+}, we have also studied the intensity of the emissions at 549 nm and 665 nm as a function of the pump power of the incident laser. It is well-known that the up-conversion intensity is directly related to the intensity of the infrared excitation by the following expression:

$$I_{UC} \propto I_{IR}{}^{n} \quad (1)$$

where n is the number of photons involved in the up-conversion process.[20,21] In Fig. 5, the logarithm UC emission intensities is plotted as a function of the logarithm of the laser pumping power for the 549 nm and 665 nm. By fitting the logarithmic curves according to eqn (1), the slope, n, obtained for the $SrSnO_3$:Er^{3+} 1% sample was 1.4 for both emissions, indicating that two photons are required in each case.

The discrepancy between the actual values of the slope (1.4) and the number of photons involved in the process (2) is due to a phenomenon described by Pollnau *et al.* as a saturation in the up-conversion process at high power, which causes the slope of the curve to gradually decrease as the laser power increases.[22] According to this interpretation, a high pump power would increase the competition between linear decay and up-conversion for the depletion of the intermediate excited states, resulting in a substantially reduced slope.

Finally, the dynamics of the 549 nm emission was studied by measuring the corresponding temporal evolution under excitation at 975 nm (see Fig. 6). In this case, a rapid rise time is observed after excitation with the laser, followed by a rapid decline. This behavior is indicative of the GSA/ESA mechanism for the UC process in which, after excitation by a pulsed laser at

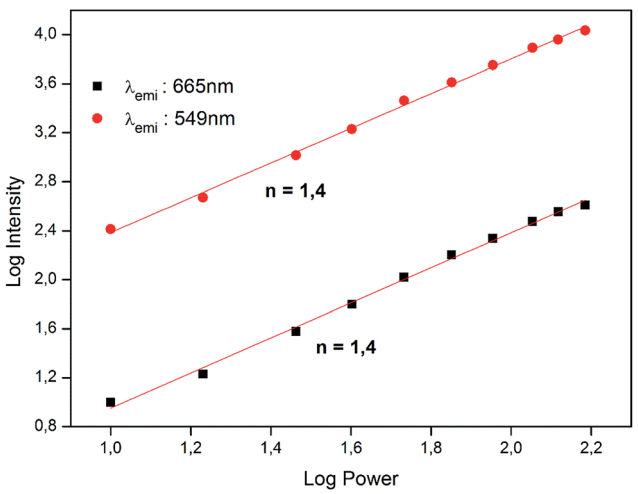

Fig. 5 Logarithm plot for the dependence of up-conversion emission intensities of the 549 and 665 nm bands on pump power at 975 nm.

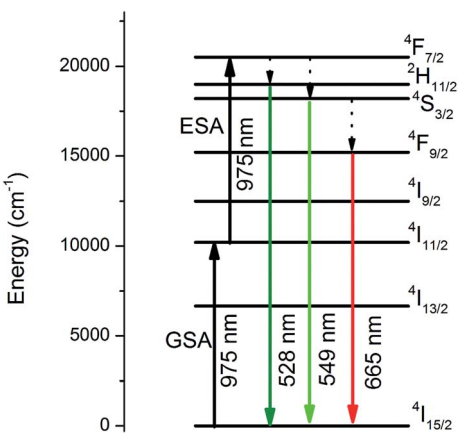

Fig. 7 Energy level diagram of Er^{3+} ion, and the possible up-conversion process.

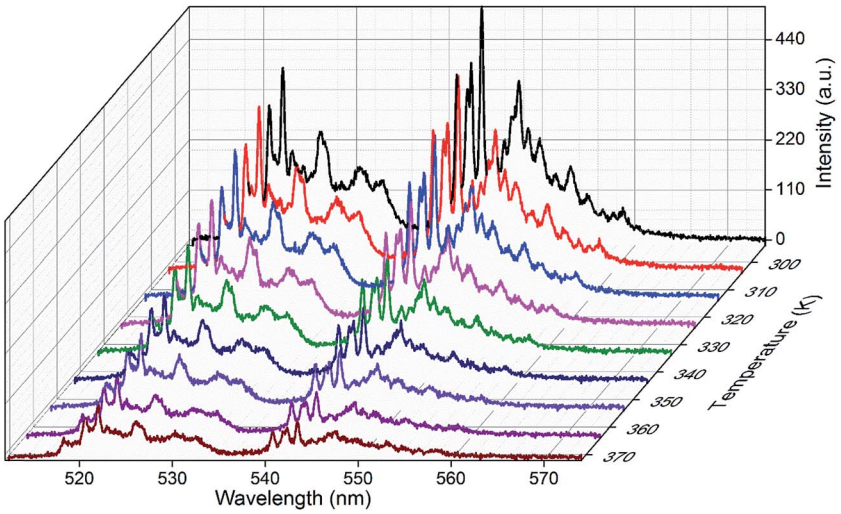

Fig. 8 Green up-conversion spectrum of $SrSnO_3$:Er^{3+} phosphor at different temperatures.

975 nm, the Er^{3+} ion is immediately excited to the $^4I_{11/2}$ level by absorbing a photon and then to the $^4F_{7/2}$ level by absorbing a second 975 nm photon. In this process, the population of the $^4F_{7/2}$ level increases rapidly as a result of successive two-photon absorption, similar to the population that could be observed, if this level was directly excited. Subsequently, a non-radiative relaxation occurs from the $^4F_{7/2}$ level to the $^2H_{11/2}$ and $^4S_{3/2}$ levels, which generates the emissions at 528 nm and 549 nm. Therefore, as shown in Fig. 6, there is an immediate rise time after the pulse excitation at 975 nm, confirming the proposed UC mechanism. On the other hand, due to their small energy gap, Er^{3+} ions in the $^4S_{3/2}$ state rapidly relax to the $^4F_{9/2}$ levels through a non-radiative process, from which they radiatively relax to the $^4I_{15/2}$ ground state emitting a red photon (665 nm). The mechanism is shown in Fig. 7.

3.5. Temperature sensing study

To investigate the optical temperature sensing behavior of the $SrSnO_3$ phosphor doped with Er^{3+}, the UC spectra, as shown in Fig. 8, were recorded using a 975 nm excitation over the range of 510–580 nm while increasing the temperature from 294 to 372 K. This temperature range is interesting for biological processes. The spectra show that the integrated intensity of both green emission bands, assigned to the $^2H_{11/2} \rightarrow {}^4I_{15/2}$ and $^4S_{3/2} \rightarrow {}^4I_{15/2}$ transitions of the Er^{3+} ion at 528 nm and 549 nm, respectively, do not change position as a function of temperature. Furthermore, the emission intensity of both bands shows an obvious dependence on the temperature. The relative intensity of the $^2H_{11/2} \rightarrow {}^4I_{15/2}$ transition increases with an increase in temperature, respect to the $^4S_{3/2} \rightarrow {}^4I_{15/2}$ transition. It is well-known that the energy gap between the $^2H_{11/2}$ and $^4S_{3/2}$ levels is quite small (200–2000 cm^{-1}).[23] Because of this small separation, the $^2H_{11/2}$ level can be easily populated from the $^4S_{3/2}$ level by thermal agitation, resulting in the variation of the emission intensity of the $^2H_{11/2} \rightarrow {}^4I_{15/2}$ and $^4S_{3/2} \rightarrow {}^4I_{15/2}$ transitions as the temperature increases.[4]

3.5.1. Fluorescence intensity ratio (FIR) and sensor sensitivity (S). As stated previously, the $^2H_{11/2}$ and $^4S_{3/2}$ levels are thermally coupled and the transition from these two levels to the ground state can be used for optical thermometry using the FIR or R technique[8] and, according to the Boltzmann distribution theory, the FIR can be expressed by the following equation:

$$\mathrm{FIR} = \mathrm{R} = \frac{I_{528}}{I_{549}} = A\exp\left(-\frac{\Delta E}{k_B T}\right) \quad (2)$$

where I_{528} and I_{549} are the integrated intensities of the $^2H_{11/2} \rightarrow {}^4I_{15/2}$ and $^4S_{3/2} \rightarrow {}^4I_{15/2}$ transitions, respectively, ΔE is the energy gap between the $^2H_{11/2}$ and $^4S_{3/2}$ levels, A is a constant, k_B is the Boltzmann constant and T is the absolute temperature.[3]

Following eqn (2), the $\ln(I_{528}/I_{549})$ was plotted against the inverse absolute temperature ($1/T$), as shown in Fig. 9. All the experimental data points were fit to a line, which had a slope of -836.07 ± 4.49 and an intercept of 2.52 ± 0.01, to determine the energy gap, ΔE, of the two thermally coupled levels and the

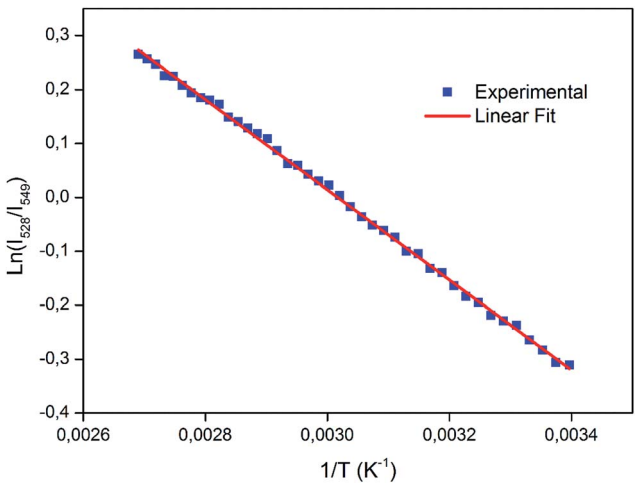

Fig. 9 Plot of the logarithmic of FIR (I_{528}/I_{549}) *versus* inverse of absolute temperature.

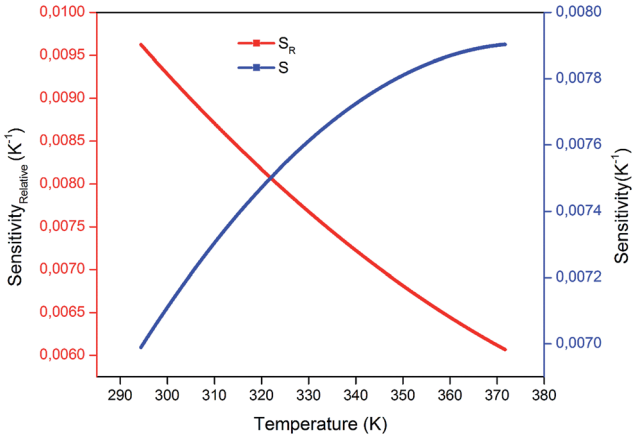

Fig. 10 Variation of sensor sensitivity and relative sensor sensitivity as a function of temperature.

coefficient, A, which were 581.09 cm^{-1} and 12.4, respectively. For a better understanding of the performance and the applicability of this material, it is also important to consider the detection sensitivity (S), which is calculated using the following formula:[24]

$$S = \left|\frac{dR}{dT}\right| = R\left(\frac{\Delta E}{k_B T^2}\right) \quad (3)$$

Alternatively, the relative temperature sensitivity (S_R) is another key parameter for sensing applications. S_R is used to compare broad categories of temperature sensors and can be expressed as:[9,25]

$$S_R = \left|\frac{1}{R}\frac{dR}{dT}\right| = \left(\frac{\Delta E}{k_B T^2}\right) \quad (4)$$

The calculated values obtained from eqn (3) and (4) were plotted as a function of absolute temperature as shown in Fig. 10. The maximum detection sensitivity (S) has a value of 7.91×10^{-3} K^{-1} at 368 K, whereas the maximum relative sensitivity (S_R) is 9.97×10^{-3} K^{-1} at 294 K. Table 2 shows a comparison of the maximum relative sensor sensitivities, used in optical thermometry, from different synthesized materials. As shown, $SrSnO_3$ has not yet been reported for optical thermometry, but $SrSnO_3$ is comparable to other synthesized materials, with a sensitivity that is similar to the previously reported values.

Table 2 Relative sensitivity for FIR-based optical temperature sensors in different host materials

Sensing materials	Relative sensitivity (K^{-1})	Temperature range (K)	Reference
Er^{3+}:$SrSnO_3$	$836.7/T^2$	294–372	This work
Er^{3+}/Yb^{3+}:$SrMoO_4$	$979.8/T^2$	93–773	4
Er^{3+}:germanate glass	$918.6/T^2$	300–600	9
ZnO:Er^{3+} nanocrystals	$880/T^2$	273–573	21
Er^{3+}/Yb^{3+}:silicate glass	$592.6/T^2$	296–723	26
Er^{3+}/Yb^{3+}:La_2O_3 phosphor	$814.4/T^2$	303–600	27
Er-Mo:$Yb_2Ti_2O_7$ nanophoshor	$679.2/T^2$	290–610	28
Er^{3+}:fluorotellurite glass	$755/T^2$	100–573	29
Er^{3+}/Yb^{3+}:Gd_2O_3 nanophosphor	$746.4/T^2$	300–900	30
YF:Er^{3+}/Yb^{3+} nano/micro crystals	$997.4/T^2$	260–490	31

The as-prepared up-conversion phosphors could be used as temperature sensors in biological systems. This is in good agreement with the results reported by Suo *et al.*[31] where similar systems were used as temperature sensors in *ex vivo* experiments at sub-tissue level. It is know that's micron-sized agglomerates are unappropriated for biological applications. More work in order to obtain particles of nanometric-size is in progress.

4. Conclusions

$SrSnO_3$ doped with Er^{3+} was successfully synthesized using a sol–gel method. Powder XRD characterization showed that the structure crystalized as a distorted orthorhombic perovskite of space group *Pbnm*. The cell volume and the lattice parameters showed that the substitution of the Er^{3+} ions into the Sn^{4+} sites increase with an increase in the Er^{3+} concentration, which is in good agreement with previously reported results.

The upconversion emission spectra are dominated by the emissions at 528 nm and 549 nm. These emissions originate from the thermally coupled levels ($^2H_{11/2}$, $^4S_{3/2}$). A detailed analysis shows that the emission at 549 nm is the result of a successive, two-photon absorption of the 975 nm radiation. Furthermore, the decay curve of the emission at 549 nm from excitation at 975 nm is in good agreement with the GSA/ESA mechanism.

The synthetized phosphors can be used in the fabrication of a temperature sensor probe to monitor the temperature within the range of 294–372 K interesting for *ex vivo* biological experiments in cell cultures or tissues. The maximum sensitivity is 7.91×10^{-3} K^{-1} at 368 K and the relative sensor sensitivity is 9.97×10^{-3} K^{-1} at 294 K.

Conflicts of interest

The are no conflicts to declare.

Acknowledgements

The authors acknowledge Conicyt-Chile and Fondecyt (Grant 1130248) for their financial support. I. R. Martin acknowledges MINECO and EU-FEDER (projects MAT2015-71070-REDC and MAT2016-75586-C4-4-P). M. V. acknowledges Conicyt-Chile for a doctoral fellowship. The authors acknowledge Dr Rodrigo Castillo for helpful discussion and UCN for financial support.

References

1 J. Cao, F. Hu, L. Chen, H. Guo, C. Duan and M. Yin, Optical thermometry based of up-conversion luminescence behavior

of Er^{3+}-doped KYb_2F_7 nano-crystals in bulk glass ceramics, *J. Alloys Compd.*, 2017, **693**, 326.

2 C. D. S. Brites, A. Millán and L. D. Carlos, Lanthanides in Luminescent Thermometry, in *Handbook on the Physics and Chemistry of Rare Earths*, ed. J. C. Bunzli and V. K. Pecharsky, North Holeng, 2016, Vol. 49, p. 339.

3 X. Cheng, K. Yang, J. Wang, L. Yang and X. Cheng, Up-conversion luminescence and optical temperature sensing behavior of Yb^{3+}/Er^{3+} codoped $CaWO_4$ material, *Opt. Mater.*, 2016, **58**, 449.

4 P. Du, L. Luo and J. S. Yu, Infrared-to-visible upconversion emission of Er^{3+}/Yb^{3+}-codoped $SrMoO_4$ phosphors as wide-range temperature sensor, *Curr. Appl. Phys.*, 2015, **15**, 1576.

5 S. Jiang, P. Zeng, L. Liao, S. Tian, H. Guo, Y. Chen, C. Duan and M. Yin, Optical thermometry based on upconverted luminescence in transparent glass ceramics containing $NaYF_4$:Yb^{3+}/Er^{3+} nanocrystals, *J. Alloys Compd.*, 2014, **617**, 538.

6 X. Wang, J. Zheng, Y. Xuan and X. Yan, Optical temperature sensing of $NaYbF_4$:Tm^{3+} SiO_2 core-shell micro-particles induced by infrared excitation, *Opt. Express*, 2013, **21**, 18.

7 X. Tian, X. Wei, Y. Chen, C. Duan and M. Yin, Temperature sensor based on ladder-level assisted thermal coupling and thermal-enhanced luminescence in $NaYF_4$:Nd^{3+}, *Opt. Express*, 2014, **22**, 24.

8 D. Manzani, J. F. S. Petruci, K. Nigoghossian, A. A. Cardoso and S. J. L. Ribeiro, A portable luminescent thermometer based on green up-conversion emission of Er^{3+}/Yb^{3+} co-doped tellurite glass, *Sci. Rep.*, 2017, **7**, 41596.

9 W. A. Pisarski, J. Pisarska, R. Lisiecki and W. Ryba-Romanowski, Er^{3+}/Yb^{3+} co-doped lead germanate glasses for up-conversion luminescence temperature sensors, *Sens. Actuators, A*, 2016, **252**, 54.

10 S. Ouni, S. Nouri, J. Rohlicek and R. Ben Hassen, Structural and electrical properties of the sol-gel prepared $Sr_{1-x}Er_xSnO_{3-\delta}$ compounds, *J. Solid State Chem.*, 2012, **192**, 132.

11 C. P. Udawatte, M. Kakihana and M. Yoshimura, Low temperature synthesis of pure $SrSnO_3$ and the $(Ba_xSr_{1-x})SnO_3$ solid solution by the polymerized complex method, *Solid State Ionics*, 2000, **128**, 217.

12 S. D. Shannon, Revised effective ionic radii and systematic studies of interatomic distances in alloys and chalcogenides, *Acta Crystallogr., Sect. A: Cryst. Phys., Diffr., Theor. Gen. Crystallogr.*, 1976, **32**, 751.

13 V. M. Goldschmidt, Gesetze der Krystallochemie, *Die Naturwissenschaften*, 1926, **21**, 477.

14 A. Le Bail, Whole powder patter decomposition methods and application: a retrospection, *Powder Diffr.*, 2005, **20**, 316.

15 A. Le Bail, H. Duroy and J. L. Fourquet, Ab-initio structure determination of $LiSbWO_6$ by X-ray powder diffraction, *Mater. Res. Bull.*, 1988, **23**, 447.

16 V. Petricek, M. Dusek and L. Palatinus, Crystallographic computing system JANA2006: general features, *J. Crystallogr.*, 2014, **229**, 345.

17 M. Muralidharan, V. Anbarasu, A. E. Perumal and K. Sivakumar, Room temperature ferromagnetism in Cr doped $SrSnO_3$ perovskite system, *J. Mater. Sci.: Mater. Electron.*, 2017, **28**, 4125.

18 M. C. F. Alves, S. C. Souza, M. R. S. Silva, E. C. Paris, S. J. G. Lima, R. M. Gomes, E. Longo, A. G. de Souza and I. M. G. dos Santos, Thermal analysis applied in the crystallization study of $SrSnO_3$, *J. Therm. Anal. Calorim.*, 2009, **97**, 179.

19 S. Tabanli, G. Eryurek and B. D. Bartolo, White light emission from Er_2O_3 nano-powder excited by infrared radiation, *Opt. Mater.*, 2017, **69**, 207.

20 B. M. van der Ende, L. Aarts and A. Meijerink, Lanthanide ions as spectral converters for solar cells, *Phys. Chem. Chem. Phys.*, 2009, **11**, 11081.

21 W. Yu, Y. Tian, M. Xing, Y. Fu, H. Zhang and X. Luo, Up-conversion luminescence of $NaY(WO_4)_2$: Yb, Er under 1550 and 980 nm excitation, *Mater. Res. Bull.*, 2016, **80**, 223.

22 M. Pollnau, D. R. Gameli, S. R. Lüthi, H. U. Güdel and M. P. Helen, Power dependence of upconversion luminescence in lanthanide and transition-metal-ions systems, *Phys. Rev. B: Condens. Matter Mater. Phys.*, 2000, **61**, 3337.

23 A. Pandey, V. K. Rai, V. Kumar, V. K. Kumar and H. C. Swart, Upconversion based temperature sensing ability of Er^{3+}-Yb^{3+} codoped $SrWO_4$: an optical heating phosphor, *Sens. Actuators, B*, 2015, **209**, 352.

24 A. K. Soni and V. K. Rai, Thermal and pump power effect in $SrMoO_4$:Er^{3+}-Yb^{3+} phosphors for thermometry and optical heating, *Chem. Phys. Lett.*, 2017, **667**, 226.

25 X. Wang, X. Kong, Y. Yu, Y. Sun and H. Zhang, Effect of Annealing on Upconversion Luminescence of ZnO:Er^{3+} Nanocrystals and High Thermal Sensitivity, *J. Phys. Chem. C*, 2007, **41**, 111.

26 C. Li, B. Dong, S. Li and C. Song, Er^{3+}-Yb^{3+} co-doped silicate glass for optical temperature sensor, *Chem. Phys. Lett.*, 2007, **443**, 426.

27 R. Dey and V. K. Rai, Yb^{3+} sensitized Er^{3+} doped La_2O_3 phosphor in temperature sensors and display devices, *Dalton Trans.*, 2014, **43**, 111.

28 B. S. Cao, Y. Y. He, Z. Q. Feng, Y. S. Li and B. Dong, Optical temperature sensing behavior of enhanced green upconversion emissions from Er-Mo:$Yb_2Ti_2O_7$ nanophosphor, *Sens. Actuators, B*, 2011, **159**, 8.

29 S. F. L. Luis, U. R. R. Mendoza, I. R. Martín, E. Lalla and V. Lavín, Effects of Er^{3+} concentration on thermal sensitivity in optical temperature fluorotellurite glass sensors, *Sens. Actuators, B*, 2013, **176**, 1167.

30 S. K. Singh, K. Kumar and S. B. Rai, Er^{3+}/Yb^{3+} codoped Gd_2O_3 nano-phosphor for optical thermometry, *Sens. Actuators, A*, 2009, **149**, 16.

31 H. Suo, X. Zhao, Z. Zhang, T. Li, E. M. Goldys and C. Guo, Constructing Multiform Morphologies of YF:Er^{3+}/Yb^{3+} Up-conversion Nano/Micro-crystals towards Sub-tissue Thermometry, *Chem. Eng. J.*, 2017, **313**, 65.

